nature immunology

Dendritic cells enter lymph vessels by hyaluronan-mediated docking to the endothelial receptor LYVE-1

Louise A Johnson[1], Suneale Banerji[1], William Lawrance[1], Uzi Gileadi[1], Gennaro Prota[1], Kayla A Holder[1], Yaowaluck M Roshorm[2], Tomáš Hanke[3,4], Vincenzo Cerundolo[1], Nicholas W Gale[5] & David G Jackson[1]

Trafficking of tissue dendritic cells (DCs) via lymph is critical for the generation of cellular immune responses in draining lymph nodes (LNs). In the current study we found that DCs docked to the basolateral surface of lymphatic vessels and transited to the lumen through hyaluronan-mediated interactions with the lymph-specific endothelial receptor LYVE-1, in dynamic transmigratory-cup-like structures. Furthermore, we show that targeted deletion of the gene *Lyve1*, antibody blockade or depletion of the DC hyaluronan coat not only delayed lymphatic trafficking of dermal DCs but also blunted their capacity to prime CD8$^+$ T cell responses in skin-draining LNs. Our findings uncovered a previously unknown function for LYVE-1 and show that transit through the lymphatic network is initiated by the recognition of leukocyte-derived hyaluronan.

Afferent lymphatic vessels are essential conduits for the transport of antigen-presenting DCs from the periphery to draining LNs. During normal homeostasis, low-level trafficking of immature tissue-resident DCs allows for local immune surveillance, whereas in inflammation and infection, the enhanced migration of both resident and monocyte-derived DCs allows for the efficient generation of primary immune responses to invading pathogens[1].

The first key steps in this chain of events are the migration of DCs within the tissue interstitium toward initial lymphatic capillaries, transit across the endothelium into the vessel lumen, and crawling in the direction of downstream lymphatic collectors[2]. These processes are directed by a combination of interstitial flow[3], chemotaxis and haptotaxis in response to gradients of lymphatic endothelial-derived chemokines including CCL21, CXCL12 and CX3CL1 that engage with their respective cognate leukocyte receptors CCR7, CXCR4 and CX3CR1 (refs. 4–11) and semaphorins[12]. However, the mechanisms underlying DC transit across lymphatic endothelium are poorly understood.

It is now appreciated that initial lymphatic capillaries have specialized interendothelial junctions that are distinct from those of blood capillaries[13]. These consist of loose, overlapping flaps anchored on their sides by 'buttons' that contain the adherens junction molecule VE-cadherin and tight-junction-associated proteins such as claudins and ZO-1. Notably, the openings formed by these flaps constitute 1–2-μm valve-like portals that are just large enough for migrating leukocytes to enter. Indeed, endogenous major histocompatibility complex class II (MHCII)-positive DCs have been observed to squeeze through such junctions into lymphatic capillaries[13]. Nevertheless, the interactions between DCs and lymphatic endothelium that facilitate transit remain unknown. Some previous studies have reported that transit does not involve conventional integrin-based adhesion and is instead mediated through contractile forces[5,14], whereas others have shown that in inflammation, transit requires the engagement of DC integrins with their endothelial ligands ICAM-1 and VCAM-1 (refs. 15–17). Several other candidate adhesion molecules have also been reported to regulate DC entry to the lymphatics, including CD31, CD99, CD137, L1CAM, ALCAM, and the scavenger receptors CLEVER-1 and mannose receptor[9,18,19]. However, these are also expressed in blood vessel endothelium, and no adhesion molecules specific to lymphatic entry have been convincingly described.

One particularly abundant component of button-like lymphatic junctions that has been proposed to mediate leukocyte entry is the lymphatic-vessel endothelial protein LYVE-1, a receptor for the large ubiquitous glycosaminoglycan polymer hyaluronan (HA), [GlcNAcβ1-4GlcUAβ1-3]n[20]. LYVE-1 is present at high density in the distinctive overlapping junctions of initial lymphatics but is largely absent from the conventional tight junctions of larger collector vessels. Furthermore, LYVE-1 is closely related to the primary leukocyte HA receptor CD44, which mediates HA-dependent adhesion and the extravasation of leukocytes across inflamed blood vessels[21].

Here we explored the involvement of LYVE-1 and its ligand HA in the trafficking of leukocytes within lymphatic vessels. Using *Lyve1*$^{-/-}$ mice and function-blocking monoclonal antibodies (mAbs), we found that efficient lymphatic trafficking of DCs from inflamed skin was dependent on LYVE-1, and that LYVE-1–HA interactions mediated an initial vessel entry step that was rate-limiting for DC-primed immune responses in draining LNs. Moreover, we demonstrate that migrating DCs assembled an endogenous HA surface coat, which enabled docking to the lymphatic endothelium via LYVE-1 within

[1]MRC Human Immunology Unit, Weatherall Institute of Molecular Medicine, John Radcliffe Hospital, University of Oxford, Oxford, UK. [2]Division of Biotechnology, School of Bioresources and Technology, King Monkut's University of Technology, Thonburi, Thailand. [3]The Jenner Institute, University of Oxford, Oxford, UK. [4]International Research Centre for Medical Sciences, Kumamoto University, Kumamoto, Japan. [5]Regeneron Pharmaceuticals, Tarrytown, New York, USA. Correspondence should be addressed to D.G.J. (david.jackson@imm.ox.ac.uk) or L.A.J. (louise.johnson@imm.ox.ac.uk).

Received 12 December 2016; accepted 24 April 2017; published online 15 May 2017; corrected online 2 June 2017 (details online); doi:10.1038/ni.3750

discrete 'transmigratory cups' that enveloped the transiting DC and facilitated its passage to the vessel lumen. These findings identify an important immunological function for this widely used lymphatic marker and reveal a previously unidentified role for the LYVE-1–HA interaction, as a regulator of leukocyte trafficking in the lymphatics.

RESULTS

Lyve1 deletion impairs DC migration to skin-draining LNs

To explore the involvement of LYVE-1 in the migration of DCs from the peripheral tissues to lymph during both normal homeostasis and inflammation, we used a mouse skin contact-hypersensitivity model in which sensitization with the chemical allergen oxazolone induces the rapid mobilization of epidermal Langerhans cells and dermal DCs, and subsequent trafficking to skin-draining LNs that is detectable within 24 h (**Supplementary Fig. 1a**)[22]. We observed a reduction in the number of skin-derived CD11c$^+$FITC$^+$ DCs recovered in draining inguinal and axillary LNs at 6 h and 24 h after oxazolone sensitization in *Lyve1*$^{-/-}$ BALB/c mice compared with that in *Lyve1*$^{+/+}$ littermates, followed by a compensatory increase in the number of CD11c$^+$FITC$^+$ DCs arriving at LNs at 48 h (**Fig. 1**). This interruption in trafficking was highly reproducible and seemed to affect all subsets of migratory CD11c$^+$MHCII$^+$FITC$^+$ DCs, including CD11b$^+$ DCs, CD103$^+$ DCs, EpCAM$^+$ DCs and langerin$^+$ DCs (**Supplementary Fig. 1b**,**c**).

The compositions of the leukocyte populations in the LNs of unchallenged *Lyve1*$^{-/-}$ and *Lyve1*$^{+/+}$ BALB/c mice were almost identical (**Supplementary Fig. 2**), which indicated a defect in inflammation-associated trafficking rather than in the steady-state composition of LNs in the *Lyve1*$^{-/-}$ mice. In *Lyve1*$^{-/-}$ C57BL/6 mice, we also observed a less marked, but statistically significant, reduction in DC accumulation in LNs at 6 h after oxazolone sensitization compared with that in *Lyve1*$^{+/+}$ littermates, and a similar, nonsignificant trend at 24 h, as well as a rebound at 48 h after sensitization (**Supplementary Fig. 3a–c**). In contrast, the original analysis of *Lyve1*$^{-/-}$ C57BL/6 mice did not show a migration defect[23], probably because of the incomplete nature of those initial studies. However, similar to the original analysis[23], we detected no obvious differences in gross lymphatic vessel or junctional ultrastructure in *Lyve1*$^{-/-}$ mice compared with that in *Lyve1*$^{+/+}$ littermates on either background. These initial results indicated that LYVE-1 contributed to DC migration via dermal lymphatics.

Deficient DC entry to afferent dermal lymphatics in *Lyve1*$^{-/-}$ mice

LYVE-1 is expressed on both luminal and basolateral surfaces of lymph vessel endothelium[24]. To investigate whether the delay in DC trafficking between skin and draining inguinal or axial LNs in *Lyve1*$^{-/-}$ mice is due to a defect in initial lymphatic vessel entry or subsequent intraluminal migration, we visualized the transit of

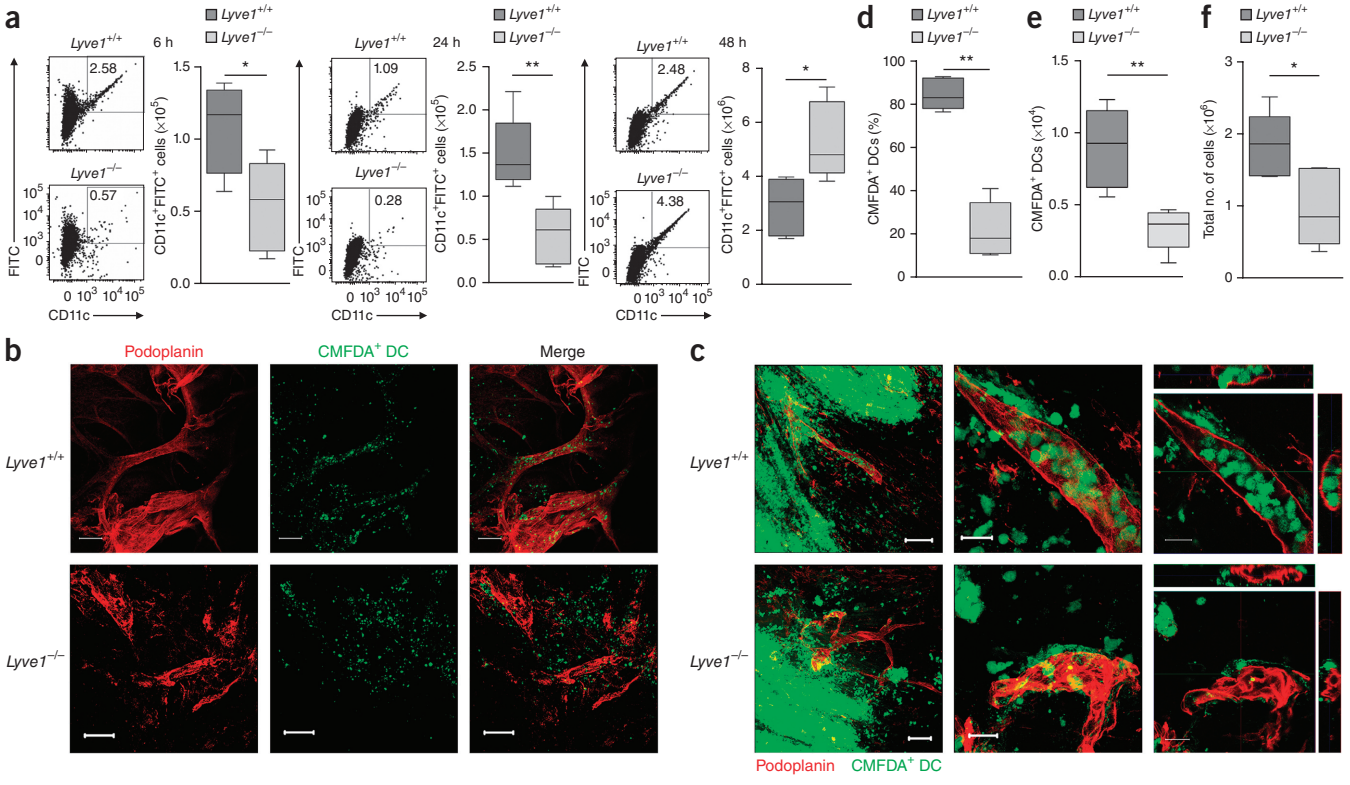

Figure 1 Impaired entry of DCs to dermal lymphatic vessels in BALB/c *Lyve1*$^{-/-}$ mice. (**a**) Recovery of endogenous DCs from draining inguinal and axillary LNs at the indicated time points after topical application of oxazolone and FITC, as measured by flow cytometry. Data in box plots represent the mean (center bar) ± s.e.m. (whiskers) ($n = 5$). Number adjacent to outlines in dot plots indicate the percentage of cells in the gate. (**b**,**c**) Entry of CMFDA-labeled BMDCs into podoplanin$^+$ afferent lymphatics of *Lyve1*$^{-/-}$ and *Lyve*$^{+/+}$ littermates, as observed by confocal microscopy of whole mount sections of ear dermis 18 h (**b**) or 24 h (**c**) after topical application of oxazolone and intradermal injection of BMDCs. Representative images from three separate repeated experiments are shown. Scale bars, 100 μm. (**c**) Three-dimensional rendering of *z*-stacks at low magnification (left; 250×) and higher magnification (middle; 630×) and including orthogonal sections (right). (**d**) Numbers of BMDCs inside the lumens of lymphatic vessels, expressed as a percentage of the number of lymphatic-vessel-associated BMDCs. Data are the mean ± s.e.m. ($n = 5$ mice). (**e**,**f**) Recovery of intradermally injected BMDCs (**e**) and overall cellularity (**f**) in draining cervical LNs 24 h after topical application of oxazolone and adoptive transfer of BMDCs, as measured by flow cytometry. Data represent the mean ± s.e.m. ($n = 5$). $^*P < 0.05$, $^{**}P < 0.01$, Mann-Whitney *U*-test. Data in box plots are from one experiment representative of three (**a**,**d**) or two (**e**,**f**) separate experiments.

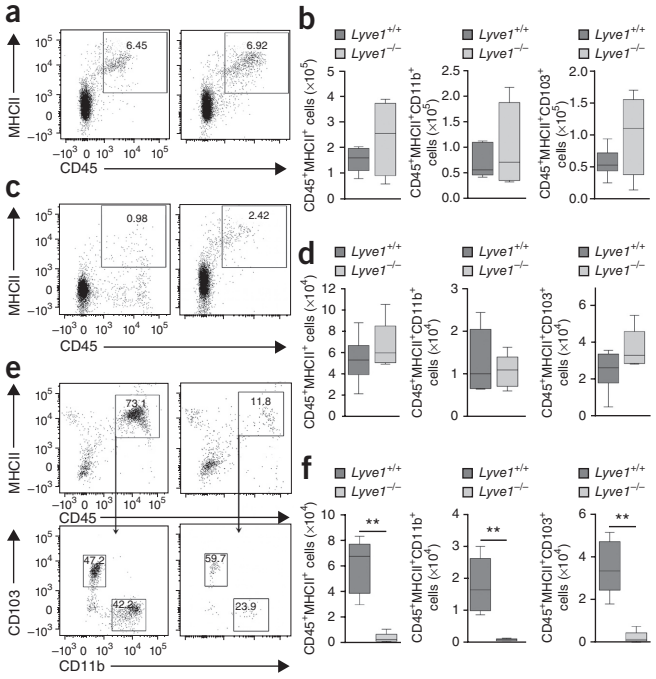

Figure 2 Impaired egress of dermal DCs from *ex vivo* cultured split ear tissue of BALB/c *Lyve1*$^{-/-}$ mice. (**a**–**d**) Flow cytometric analysis of digested ear tissue from wild-type *Lyve1*$^{-/-}$ mice and *Lyve*$^{+/+}$ littermates, either freshly resected (**a**,**b**) or after *ex vivo* culture for 24 h (**c**,**d**). (**e**,**f**) Flow cytometry analysis of cells that egressed from the dermis into the tissue culture medium. Data in box plots (**b**,**d**,**f**) represent the mean (center bar) ± s.e.m. (whiskers) ($n = 5$). Data in all plots are from one experiment representative of three different experiments. Numbers in boxes in dot plots indicate the percentage of cells in the gate. $^{**}P < 0.01$, Mann-Whitney *U*-test.

bone-marrow-derived DCs (BMDCs) through dermal lymphatics by confocal imaging. In oxazolone-sensitized *Lyve1*$^{-/-}$ and *Lyve1*$^{+/+}$ littermate mice injected with LPS-activated, CMFDA-labeled BMDCs, the cells were still visible in large numbers near the injection site 24 h after injection (**Fig. 1c**), in agreement with reports that only approximately 1% of intradermally injected BMDCs reach draining LNs within this time frame[4]. In *Lyve1*$^{+/+}$ BALB/c mice, CMFDA^{+} BMDCs were distributed along podoplanin-stained dermal lymphatic vessels at 18 h and 24 h (**Fig. 1b**,**c**), and orthogonal views of *z*-stacks showed that the majority (85%) of CMFDA^{+} cells associated with these lymphatics were inside the vessel lumen (**Fig. 1c**,**d**). In contrast, the distribution of CMFDA^{+} BMDCs in LYVE-1-deficient mice was largely independent of podoplanin^{+} lymphatics at 18 h (**Fig. 1b**), and cells associated with podoplanin^{+} lymphatics accumulated at the basolateral surface of the vessels, with only 22% present in the vessel lumen at 24 h (**Fig. 1c**,**d**), which suggests that their transit was stalled in the absence of LYVE-1. Moreover, the number of dermally injected CMFDA^{+} BMDCs (3×10^3) recovered in skin-draining LNs of oxazolone-sensitized *Lyve1*$^{-/-}$ mice was threefold lower than that in *Lyve1*$^{+/+}$ littermates (9×10^3; **Fig. 1e**), and total LN cellularity was 2.5-fold lower in *Lyve1*$^{-/-}$ mice compared with *Lyve1*$^{+/+}$ littermates (**Fig. 1f**). These results indicate that LYVE-1 contributed to the ability of DCs to access the vessel lumen.

Compromised egress of DCs from *Lyve1*$^{-/-}$ dermal explants

We next used short-term (24 h) *ex vivo* crawl-out assays[25] to investigate DC trafficking in cultured skin explants from *Lyve1*$^{-/-}$ and *Lyve1*$^{+/+}$ BALB/c littermates. These assays measure the numbers of endogenous dermal DCs and epidermal Langerhans cells migrating from the skin through afferent dermal lymphatics into the culture medium after mobilization by IL-18, IL-1β and TNF released within the excised tissue[26,27]. Freshly excised skin from *Lyve1*$^{-/-}$ and *Lyve1*$^{+/+}$ littermates contained similar numbers of resident CD45^{+}MHCII^{+} leukocytes (**Fig. 2a**,**b**). However, after 24 h of *ex vivo* incubation, the number of CD45^{+}MHCII^{+} cells recovered in the medium from the *Lyve1*$^{-/-}$ explants was 17-fold lower than that from *Lyve1*$^{+/+}$ explants (**Fig. 2c**–**f**), and the *Lyve1*$^{-/-}$ cell populations contained both CD103^{+} and CD11b^{+} DCs. Overall, these results indicate a role for LYVE-1 in the egress of dermal DCs from mouse skin explants.

DC trafficking involves interaction with LYVE-1 HA-binding domain

We next investigated the consequences of blocking LYVE-1 function *in vivo* in *Lyve1*$^{+/+}$ BALB/c mice with a panel of blocking mAbs. We used in-house-generated rat anti-mouse LYVE-1 mAbs (B1/10 and C1/8)[28,29] and a commercially available antibody (mAb2125; R&D Systems) that bound epitopes in the Link domain of LYVE-1, which binds HA. All three mAbs bound both soluble LYVE-1 and LYVE-1 expressed on the surface of transfected Jurkat cells, and blocked the binding of purified high-molecular-weight HA to LYVE-1 effectively, albeit with different affinities (mAb2125 > B1/10 > C1/8) and relative potencies (IC_{50} mAb2125 < B1/10 < C1/8; **Supplementary Fig. 4a**–**c**). Binding studies with LYVE-1 site-directed mutants and mapping onto a structure-based LYVE-1 model indicated that the C1/8 and mAb2125 epitopes were most similar to each other and bracketed the predicted HA-binding cleft on the surface of LYVE-1, binding to residues Gln50 and Asn136 (ref. 30), whereas the epitope of B1/10 seemed to lie toward the opposite face, contacting residues Arg98 and Phe100 (**Supplementary Fig. 4d**).

The administration of saturating doses of either mAb2125 or C1/8 to oxazolone-sensitized *Lyve1*$^{+/+}$ BALB/c mice caused a fivefold reduction in the number of endogenous FITC-labeled (by skin painting) CD11c^{+} DCs recovered from the draining LNs at 24 h (**Fig. 3a**), along with a reduction in the number of CD45^{+} cells in LNs and of all subsets of CD11c^{+}MHCII^{+} DCs (**Supplementary Fig. 4e**) in comparison with the numbers in *Lyve1*$^{+/+}$ mice that received rat IgG. There was no significant reduction in the numbers of CD11c^{+} FITC-labeled DCs recovered from the draining LNs of mice that received saturating doses of mAb B1/10 compared with those from rat IgG–treated controls (**Supplementary Fig. 3a**), which suggested that the discrete epitope within the LYVE-1 HA-binding surface for this antibody is not involved in DC recruitment. We observed reduced accumulation of FITC^{+}CD11c^{+} DCs in the draining LNs of C1/8- and mAb2125-treated mice after 24 h in both the sensitization and challenge phases of oxazolone hypersensitivity (**Fig. 3a**,**b**), in both BALB/c and C57BL/6 mice (**Fig. 3b**,**c**). Moreover, the inhibitory effects of C1/8 and mAb2125 on DC migration were sustained over 48 h after oxazolone sensitization (**Fig. 3d**), in contrast to the transient delay in DC recruitment seen in the *Lyve1*$^{-/-}$ mice. These results suggest that DC migration in dermal lymphatics is mediated by interactions between LYVE-1 and its ligand, HA.

We then used confocal microscopy to visualize lymphatic transit in oxazolone-sensitized BALB/c *Lyve1*$^{+/+}$ mice injected with the anti-LYVE-1 mAbs C1/8, B1/10 and mAb2125 24 h after intradermal transfer of CMFDA-labeled BMDCs. C1/8 and mAb2125 caused an accumulation of CMFDA-labeled cells at the outer (basolateral) surface of the LYVE-1^{+} lymphatic capillaries compared with the distribution in rat IgG controls, whereas B1/10 had no such effect (**Fig. 3e**). Quantification of confocal images of skin sections indicated that fewer

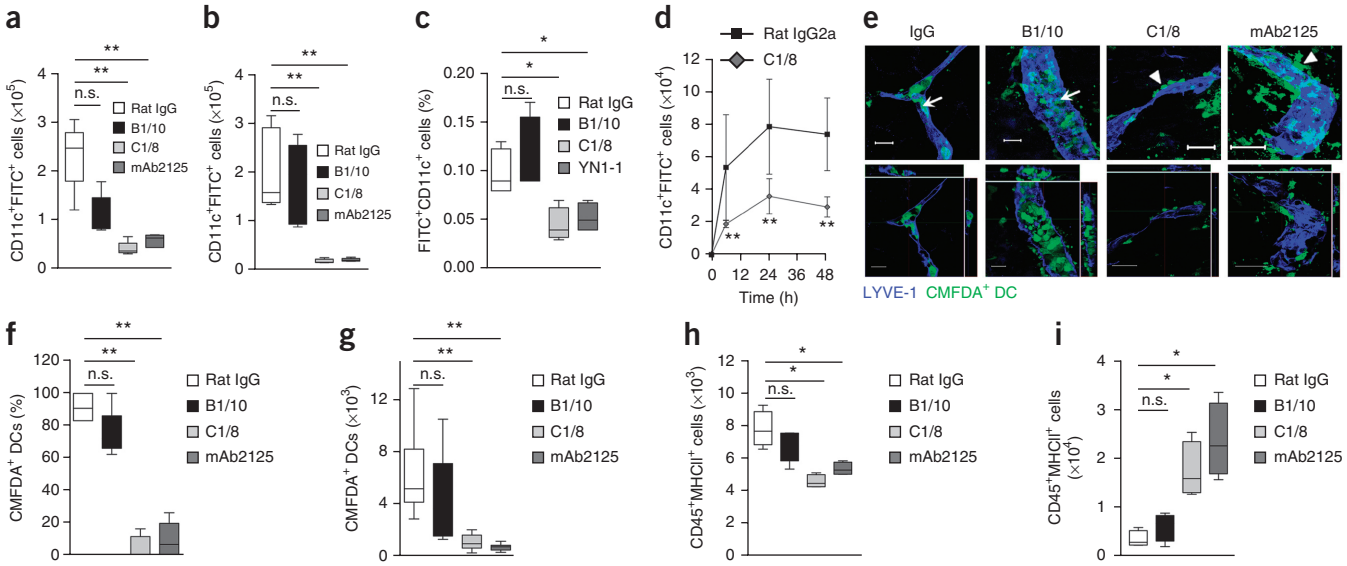

Figure 3 LYVE-1-specific mAbs inhibit *in vivo* trafficking of DCs through dermal lymphatics. (**a**,**b**) The recovery of endogenous DCs in draining LNs in BALB/c mice after injection of rat IgG or anti-LYVE-1 mAb B1/10, C1/8 or mAb2125, during either sensitization (**a**) or challenge (**b**) by topical application of oxazolone and FITC. Data show numbers of $CD45^+FITC^+CD11c^+$ DCs ($n = 5$). (**c**) The effect of anti-LYVE-1 mAbs on DC trafficking in C57BL/6 mice 24 h after skin painting with oxazolone and FITC. The anti-ICAM-1 mAb YN1-1 was used as a positive control ($n = 4$). (**d**) The recovery of DCs from draining LNs 6–48 h after topical application of oxazolone and FITC in BALB/c mice injected with rat IgG2a or C1/8 ($n = 4$). (**e**,**f**) The entry of CMFDA-labeled BMDCs into dermal afferent lymphatics immunostained with rabbit anti-LYVE-1 after oxazolone skin painting. Magnification, 630×; scale bars, 20 μm (rat IgG and B1/10) or 50 μm (C1/8 and mAb2125) (**e**). Arrows indicate BMDCs within lymphatic vessel lumens; arrowheads indicate BMDCs restricted to basolateral surfaces of vessels. Data in **f** are expressed as a percentage of lymphatic-vessel-associated BMDCs ($n = 5$). (**g**) The recovery of BMDCs from draining LNs 24 h after rat IgG or mAb injection. (**h**,**i**) Results of *ex vivo* skin crawl-out assays from ear tissue, showing numbers of egressed DCs (**h**) and remaining dermal DCs (**i**) ($n = 5$). Data in plots represent the mean ± s.e.m. n.s., not significant; $^*P < 0.05$, $^{**}P < 0.01$, Mann-Whitney *U*-test. Data are from one experiment representative of three (**a**–**c**,**e**–**i**) or two (**d**) different experiments.

than 20% of vessel-associated $CMFDA^+$ BMDCs were present within the lumen in C1/8- and mAb2125-treated mice, whereas >80% of vessel-associated $CMFDA^+$ BMDCs were intraluminal in mice treated with control IgG or B1/10 (**Fig. 3f**). In addition, treatment with C1/8 or mAb2125 elicited a fivefold reduction in the number of $CMFDA^+$ BMDCs recovered in the draining LNs of oxazolone-sensitized mice at 24 h after intradermal injection compared with numbers in rat IgG–treated controls (**Fig. 3g**).

We also investigated the effects of LYVE-1 mAb blockade on endogenous $CD45^+MHCII^+$ DC migration in dermal lymphatics of cultured BALB/c skin explants using an *ex vivo* crawl-out assay that quantifies the recovery of egressed cells in the surrounding media (supernatant) after 24 h. Treatment with C1/8 or mAb2125 over this period caused a significant 1.6-fold reduction in the number of $CD45^+MHCII^+$ cells collected from the explant supernatants compared with that from rat IgG–treated controls, whereas B1/10 had no significant effect (**Fig. 3h**). This was mirrored by a reciprocal increase in the number of $CD45^+MHCII^+$ DCs retained within the dermis in C1/8- and mAb2125-treated explants (**Fig. 3i**), which indicated that targeting of the LYVE-1–HA interaction prevents DC exit via dermal lymphatics. These results show that disruption of LYVE-1–HA interactions by LYVE-1-blocking mAbs impaired lymphatic trafficking of DCs at the point of initial vessel entry, and that similar interference reduced DC egress from dermal tissue explants.

LYVE-1-mediated DC migration promotes LN $CD8^+$ T cell responses

Next we examined the physiological importance of LYVE-1-mediated DC trafficking for antigen delivery and cell-mediated immune responses in draining LNs. We measured the effects of C1/8 and B1/10 administration on the F5 transgenic $CD8^+$ T cell response to the influenza virus A/NT/60/68 nucleoprotein (NP) peptide ASNENDAM[28,31], expressed from a modified vaccinia virus Ankara (MVA)-vectored MVA.HIVA.NP vaccine in C57BL/10 mice. Mice that underwent adoptive (intravenous) transfer with CFSE-labeled F5 T cells received intraperitoneal (i.p.) injections of LYVE-1 mAbs 24 h before and after intradermal MVA.HIVA.NP vaccination. In this model, peptide is delivered to LNs through virus uptake by migrating dermal antigen-presenting cells[28] and thus depends on the efficient migration of antigen-loaded DCs through afferent lymphatic capillaries. Administration of C1/8 reduced the number of proliferating NP-specific F5 $CD8^+$ T cells in the draining cervical LNs by more than 40% compared with that in rat IgG–treated controls, as determined by CFSE dilution 72 h after challenge, whereas B1/10, which did not block DC trafficking to skin-draining LNs, had no appreciable effect (**Fig. 4a**,**b**). Importantly, i.p. injection of C1/8 did not alter the proliferation of F5 T cells in the spleens of mice immunized intravenously with MVA.HIVA.NP compared with that in rat IgG–treated controls (**Fig. 4c**). Because the spleen lacks an afferent lymphatic supply, these results indicate that the mAbs that blocked the LYVE-1–HA interaction specifically targeted afferent lymphatic trafficking.

We also investigated the proliferative response of intravenously adoptively transferred CFSE-labeled ovalbumin-specific OT-1 $CD8^+$ T cells in the draining LNs of *Lyve1*$^{-/-}$ C57BL/6 mice and control *Lyve1*$^{+/+}$ littermate recipients after intradermal transfer of BMDCs pulsed with ovalbumin peptide *ex vivo*. We observed a 25% reduction in numbers of proliferating OT-1 $CD8^+$ T cells in the draining cervical LNs of LYVE-1-deficient mice (44.8%) compared with that in *Lyve1*$^{+/+}$ littermates (59.7%), as determined by CFSE labeling 44 h after the transfer of antigen-loaded DCs (**Fig. 4d**,**e**). Furthermore, OT-1 $CD8^+$ T cells transferred into *Lyve1*$^{-/-}$ mice showed lower expression of the

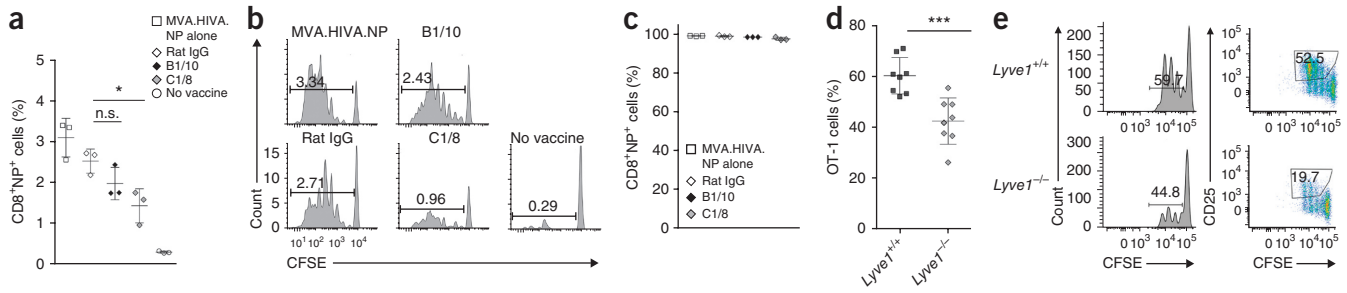

Figure 4 Disruption of LYVE-1-mediated DC trafficking inhibits primary antigen-specific T cell responses in skin-draining LNs. (**a**,**b**) Influenza-NP-specific LN CD8⁺ T cell proliferation in response to dermally injected MVA.HIVA.NP vaccine in C57BL/10 mice that had received adoptively transferred F5 transgenic T cells and injections of LYVE-1 mAbs, as determined by flow cytometry. Data in **a** represent the percentage of the total dividing F5 tetramer-reactive CD8⁺ T cells (mean ± s.e.m.). $n = 3$. (**b**) Representative histograms of CFSE fluorescence, indicating levels of LN T cell activation. (**c**) Spleen CD8⁺ F5 T cell responses in mice injected intravenously with MVA.HIVA.NP and the indicated LYVE-1 mAbs, as determined by flow cytometry. Data are the mean ± s.e.m. ($n = 3$). (**d**,**e**) Ovalbumin-specific LN CD8⁺ T cell responses elicited by peptide (SIINFEKL)-pulsed BMDCs after injection into C57BL/6 *Lyve1*$^{-/-}$ or wild-type *Lyve1*$^{+/+}$ mice that had received adoptively transferred OT-1 transgenic T cells. (**d**) LN T cell proliferation status as determined by flow cytometry, plotted as the percentage of dividing OT-1-tetramer-reactive CD8⁺ T cells. Data are the mean ± s.e.m. ($n = 8$). (**e**) Representative histograms of CFSE fluorescence and CD25 expression levels within gated cell populations, indicating levels of LN T cell activation. No CD8⁺ T cell proliferation was detected in nondraining LNs. Numbers in outlines indicate the percentage of cells in the gate. n.s., not significant; $^*P < 0.05$, Mann-Whitney *U*-test; $^{***}P < 0.005$, Student's *t*-test. Data are from one experiment representative of three (**a**–**c**) or two (**d**,**e**) experiments.

T cell–activation markers CD25 and CD69 compared with that in *Lyve1*$^{+/+}$ littermate controls (**Fig. 4e** and data not shown). We could not detect T cell proliferation or upregulation of activation markers in nondraining LNs (data not shown). These results indicate that interference with LYVE-1 blocks LN T cell proliferation in response to dermally administered peptide antigens.

LYVE-1 engages migrating DCs via their endogenous surface HA

To investigate whether DC entry to lymphatics is modulated by LYVE-1 interaction with HA on the DC surface[32,33], we first incubated BMDCs with recombinant biotin-labeled versican G1 domain (bVG1), a high-affinity HA-binding protein reagent used to detect HA on the surface of cells[34,35]. bVG1 stained approximately 50% of CD11c⁺MHCII⁺ BMDCs, as assessed by confocal microscopy and flow cytometry (**Fig. 5a**,**b** and **Supplementary Fig. 5**). Using a sensitive competitive ELISA, we also detected HA in whole-cell lysates and supernatants of both immature and LPS-activated BMDCs (**Fig. 5c**,**d**). Additionally RT-PCR showed that BMDCs expressed *Has2* mRNA, encoding the key HA synthase protein[32] (**Fig. 5e**), which suggests a capacity for endogenous HA synthesis. HA was also detected on

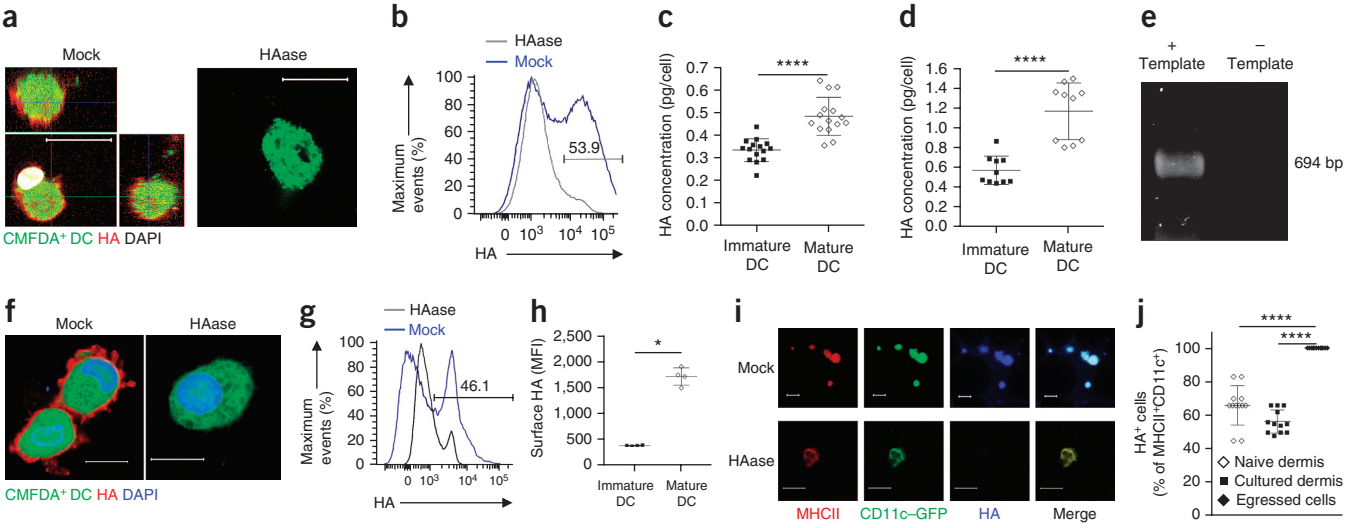

Figure 5 DCs express HA as a cell-surface coating. (**a**–**e**) HA detection. (**a**,**b**) Detection of HA in CMFDA-labeled BMDCs, with bVG1 applied after incubation in the absence (mock) or presence of HAase, as determined by confocal microscopy (**a**) and flow cytometry (**b**). HA was present in both BMDC lysates (**c**) and supernatants (**d**), both in immature cells and after LPS-induced maturation, as determined by ELISA ($n = 15$). (**e**) The expression of *Has2* mRNA in mature DCs as shown by RT-PCR. (**f**,**g**) HA on mature human CMFDA-labeled MDDCs detected with bVG1, with or without HAase (**f**), and by flow cytometry of HAase-treated control cells and mock-treated cells (**g**). (**h**) Surface HA levels before and after LPS-induced maturation; $n = 4$. MFI, mean fluorescence intensity. (**i**) Surface HA in endogenous dermal DCs in CD11c–GFP reporter mice, detected by bVG1 (blue) and immunostained with anti-MHCcIII, with or without HAase. (**j**) Results of *ex vivo* skin crawl-out assays showing the percentage of CD11c–GFP⁺MHCcIII⁺ DCs retained and egressed after 24 h in culture, scored as surface-HA⁺ by microscopy. We used four mice per condition, from which three fields of view were assessed ($n = 12$). Data in all panels are from one experiment representative of three. Data in **c**, **d**, **h** and **j** represent the mean ± s.e.m. $^*P < 0.05$, $^{****}P < 0.0001$, Mann-Whitney *U*-test. Scale bars, 10 μm.

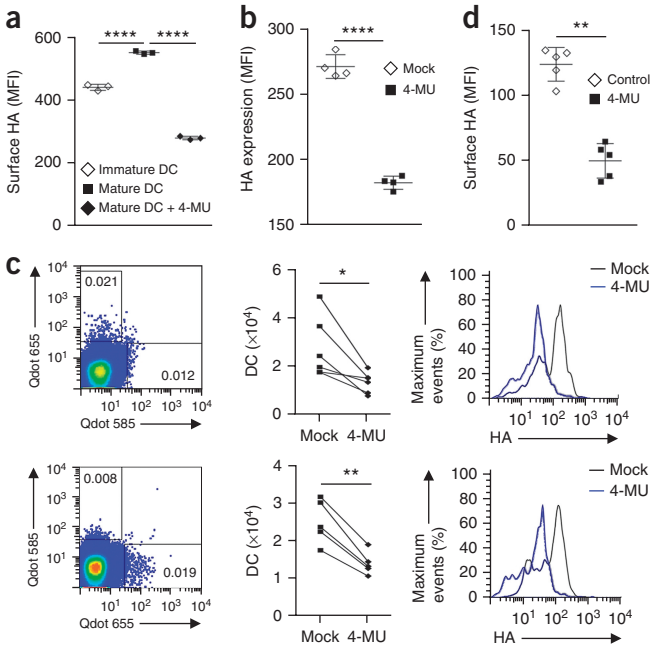

Figure 6 HA is required for efficient lymphatic migration of DCs to skin-draining LNs. (**a**,**b**) Depletion of surface HA from mature BMDCs by HAase digestion and *in vitro* culture (72 h) with or without 4-MU as assessed by streptavidin/bVG1 binding and flow cytometry. The graphs show surface HA levels on immature and mature BMDCs incubated either alone (mock) or in the presence of 4-MU (**a**) and 24 h after the end of 4-MU inhibition (**b**). Data are the mean ± s.e.m. (BMDCs from $n = 3$ mice). (**c**,**d**) Trafficking of control mock-treated and HAase/4-MU-treated BMDCs to draining LNs, quantitated by differential labeling with Qdot 655 and Qdot 585, respectively (**c**, upper row), or the reverse (bottom row), 24 h after 1:1 coinjection into the dermis of oxazolone-treated mice. The relative numbers of each BMDC population recovered from draining LNs are shown in dot plots and matched pair graphs ($n = 5$). Representative Flow cytometric histograms show the surface HA levels in Qdot-labeled HAase/4-MU treated BMDCs recovered from cervical nodes, compared with mock-treated controls. Statistical analysis was done by paired Student's *t*-test. Numbers in quadrants in dot plots indicate the percentage of cells in the respective quadrant. (**d**) Surface HA levels pooled from the samples shown in **c**. Data are the mean ± s.e.m. MFI, mean fluorescence intensity. $^*P < 0.05$, $^{**}P < 0.01$, $^{****}P < 0.0001$, Mann-Whitney *U*-test (**a**,**b**,**d**) or paired Student's *t*-test (**c**). All data are from one experiment representative of three experiments.

human monocyte-derived DCs (MDDCs) (**Fig. 5f**,**g**), and its expression increased after LPS-induced maturation (**Fig. 5h**).

To assess whether HA was expressed by tissue-resident DC populations *in vivo*, we used bVG1 to stain whole-mount tissue sections of ear skin from *Lyve1*$^{+/+}$ mice *in situ*, as well as cytospin preparations of dermal DCs egressed from dermal explants cultured for 24 h *ex vivo*. Because mAbs to CD11c failed in whole-mount staining protocols, we carried out immunostaining with anti-MHCII and bVG1 in transgenic CD11c–GFP reporter mice to identify endogenous CD11c$^+$ DCs (**Supplementary Fig. 6**). We detected HA expression on a large proportion (67%) of resident CD11c–GFP$^+$MHCII$^+$ DCs *in situ* in skin sections from these mice (**Fig. 5i**), as well as on all CD11c–GFP$^+$MHCII$^+$ DCs that had egressed from the cultured dermal explants after 24 h (**Fig. 5j**), which indicated enrichment of the glycosaminoglycan in the latter cell population.

To directly test whether HA is required for DC migration through lymphatic vessels, we depleted HA from the surface of immature BMDCs by digestion with purified hyaluronidase (HAase) and followed that with a 72-h treatment in culture with 4-methylumbelliferone (4-MU), a nontoxic HA synthase inhibitor, to prevent replenishment by *de novo* resynthesis during subsequent LPS-induced DC maturation. After this treatment, HA levels decreased to approximately 50% of those in mock-treated BMDCs, and they remained stable 24 h after the removal of 4-MU (**Fig. 6a**,**b**). However, the treatment did not significantly affect BMDC viability, surface integrin integrity or the expression of CD86, which was used as a measure of activation (**Supplementary Fig. 5c–e**). To assess the effects on lymphatic migration, we injected HAase/4-MU-treated or mock-treated BMDCs, tagged with Q-dot 585 or Q-dot 655, respectively, intradermally into oxazolone-sensitized BALB/c *Lyve1*$^{+/+}$ mice and then carried out flow cytometry to assess the numbers of labeled BMDCs in draining LNs. Twenty-four hours after cell transfer, we recovered up to threefold more mock-treated DCs than HAase/4-MU-treated DCs from draining LNs, with the latter showing decreased surface expression of HA (**Fig. 6c**,**d**). These data indicate that DCs express HA on their surface both *in vitro* and *in vivo*, and suggest that HA expression is important for trafficking via afferent lymphatics.

LYVE-1–HA interactions mediate DC adhesion and transmigration

To define the molecular mechanisms by which LYVE-1 and HA mediate DC trafficking through lymphatics, we used *in vitro* adhesion and transendothelial migration assays in which CMFDA-labeled, LPS-matured BMDCs were coincubated over monolayers of primary LYVE-1$^+$ mouse dermal lymphatic endothelial cells (mLECs) isolated from the skin of neonatal BALB/c mice by immunomagnetic bead selection with C1/8 (ref. 15) and plated on plastic multiwell dishes and on the undersurface of opaque Transwell inserts, respectively. Coincubation (2 h) with either mAb2125 or C1/8 reduced the number of BMDCs adhering to the mLEC monolayers by twofold compared with cells treated with isotype-matched control rat IgG, whereas B1/10 had no significant effect (**Fig. 7a**). Likewise, preincubation (2 h) with purified HAase reduced the number of BMDCs adhering to mLEC monolayers by more than threefold compared with mock-treated controls, whereas HAase treatment of mLECs had no such effect (**Fig. 7b**), which indicated that HA expressed by BMDCs is required for the interaction. Moreover, the inclusion of C1/8 or mAb2125 throughout the duration (12 h) of Transwell assay cultures reduced BMDC basolateral-to-luminal transmigration through the mLEC layer by twofold in each case, as assessed by quantitation of fluorescent (CMFDA) cell numbers, compared with the rat IgG–treated isotype control, whereas B1/10 showed no statistically significant effect (**Fig. 7c–e**). These results indicate that both DC adhesion and migration across a lymphatic endothelial cell (LEC) monolayer involved LYVE-1 interaction with HA on the DC surface.

Docking to lymphatic endothelium via LYVE-1 transmigratory cups

We next used high-magnification confocal microscopy of BMDCs cocultured with primary mLEC monolayers to image the DC–LEC interface and visualize how the interaction between HA and LYVE-1 facilitates adhesion and transmigration. We observed that adherent BMDCs docked to the mLEC monolayer surface in discrete ring-like structures that stained intensely for LYVE-1 (**Fig. 7f**). In *z*-stack orthogonal views of the confocal images, the ring-like structures appeared as cups that extended from the endothelium, partly enveloping the adherent DCs (**Fig. 7g**,**h**). The addition of C1/8 or mAb2125 to the mLEC–BMDC cocultures, or HAase pretreatment of the BMDCs, greatly reduced the number of LYVE-1$^+$ cups that formed on the mLEC monolayer surface compared with that in a rat IgG–treated

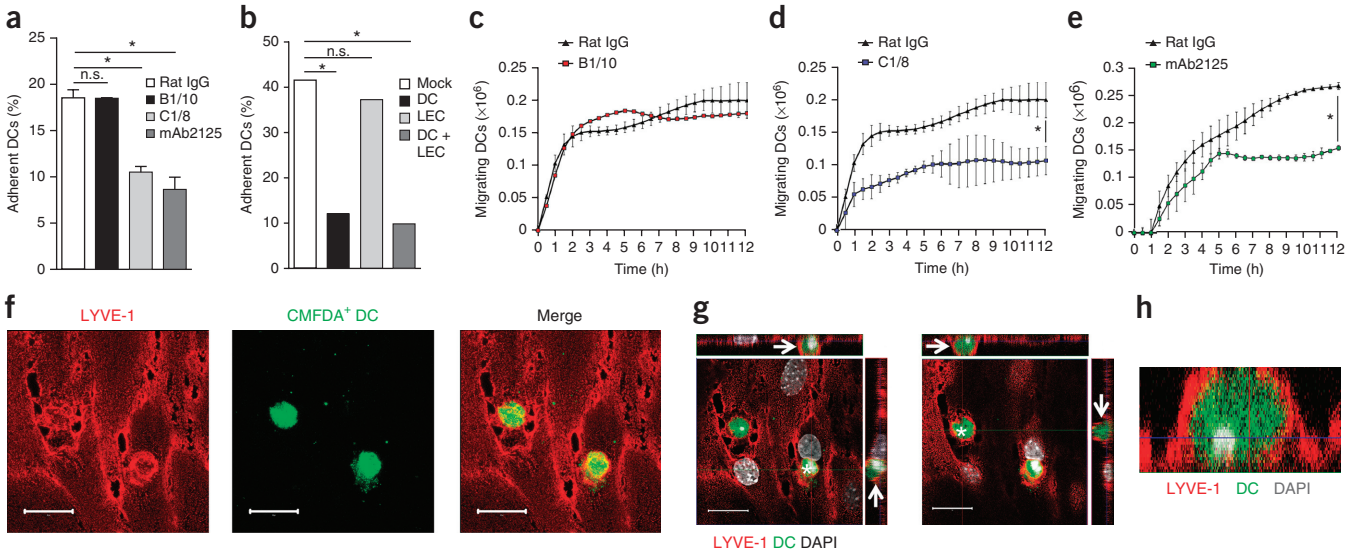

Figure 7 DCs adhere to LECs in an HA- and LYVE-1-dependent manner via LYVE-1-enriched transmigratory cups. (**a**,**b**) Adhesion of LPS-matured, CMFDA-labeled BMDCs to primary mLEC monolayers after 3 h of incubation in the presence of rat IgG or anti-LYVE-1 mAbs (**a**), or after 2 h of preincubation with HAase (**b**), as assessed by fluorescence plate reader. Data are the mean and s.e.m.; $n = 4$. (**c**–**e**) Basolateral-to-luminal transmigration of LPS-matured, fluorescently labeled BMDCs across mLEC monolayers grown on the undersurface of Transwell filters, quantitated over time by fluorescence plate reader in the presence of rat IgG, B1/10 (**c**), C1/8 (**d**) or mAb2125 (**e**). Data are the mean ± s.e.m.; $n = 4$. (**f**–**h**) Confocal microscopy images of cultured primary mLEC monolayers immunostained with rabbit anti-LYVE-1 (**f**), viewed 3 h after the addition of fluorescently labeled BMDCs (CMFDA), and counterstained with DAPI (**g**,**h**). LYVE-1-enriched cups surrounding individual DCs (asterisks) are indicated by arrows (**g**). A digital zoomed-in view of an orthogonal view is shown in **h** (magnification, 630×; scale bars, 20 μm). *$P < 0.05$, Mann-Whitney *U*-test. Data and images are from one experiment representative of three separate experiments (**a**–**h**).

isotype control (**Fig. 8a**,**b** and **Supplementary Fig. 7**), which implied that the interaction between LYVE-1 and HA on the surface of BMDCs contributes to the stability of these molecular structures. We observed similar LYVE-1$^+$ cups on primary human LEC monolayers incubated with human MDDCs (**Supplementary Fig. 7**), and their formation was inhibited by the addition of the human LYVE-1–HA-blocking mAb 891 (**Fig. 8c** and **Supplementary Fig. 7**). In addition, in frozen skin sections from oxazolone-sensitized BALB/c mice, HA was closely associated with endogenous MHCII$^+$ DCs that were undergoing transmigration into lymphatic vessels (**Fig. 8d**). Finally, in skin sections from oxazolone-sensitized mice injected intradermally with CMFDA-labeled BMDCs, these cups were observed in close contact with LYVE-1$^+$ protrusions of lymphatic vessels during diapedesis (**Fig. 8e** and **Supplementary Fig. 8**). These results show that the adhesion of DCs to LECs involved the formation of LYVE-1$^+$ endothelial transmigratory cups through interaction with DC HA, and provide evidence that these cups form both *in vitro* and *in vivo*.

DISCUSSION

Here we have shown that the endothelial HA receptor LYVE-1 is an important mediator of leukocyte trafficking. LYVE-1 promoted the docking of DCs to lymphatic vessel endothelium within dynamic endothelial transmigratory cups by engaging HA expressed by DCs[32]. By using a topical oxazolone-induced model of skin hypersensitivity in mice, *ex vivo* dermal crawl-out assays, *in vitro* transmigration assays, and fluorescent imaging, we demonstrated that genetic deletion of *Lyve1* or functional disruption by mAbs that interfere with HA–LYVE-1 interactions impaired the early transit of DCs through dermal lymphatic capillaries to draining LNs by preventing their interaction with the lymphatic endothelium. LN trafficking and the formation, adhesion and transmigration of endothelial cups were all impaired by enzymatic removal of HA from the surface of DCs and prolonged inhibition of endogenous HA biosynthesis. Lastly, *Lyve1* deletion or antibody blockade significantly reduced CD8$^+$ T cell responses to peptide antigens in LNs. Thus, LYVE-1–HA interaction mediated a rate-limiting step for DC lymphatic entry and the initiation of immune responses in skin-draining LNs.

The transient nature of the DC-trafficking defect in *Lyve1*$^{-/-}$ mice and the more sustained effects of LYVE-1 antibody blockade in adult *Lyve1*$^{+/+}$ mice suggest the existence of compensatory mechanisms during embryonic development in mice with genomic deletion of *Lyve1*, a phenomenon previously suggested for mice deficient in the primary leukocyte HA receptor CD44 (refs. 36,37). Compensation through functional redundancy may account for the apparently normal phenotype of *Lyve1*$^{-/-}$ mice under normal homeostatic conditions. Moreover, the comparatively short duration of the trafficking defects in *Lyve1*$^{-/-}$ mice, particularly those on the C57BL/6 background, provides an explanation for the failure to identify an important trafficking role for LYVE-1 in earlier, more limited studies[23]. Clearly, more detailed studies of lymphatic trafficking in mice, including live imaging and conditional or acute deletion of *Lyve1*, will be required in order for such phenomena to be fully defined in the future.

A function for LYVE-1 as a lymph-specific trafficking receptor is fully consistent with its segregated expression at the tips of the interdigitating endothelial junctions of initial lymphatic vessels, which act as hot spots for DC entry *in vivo*[13]. HA-mediated docking with LYVE-1 at these sites could facilitate DC transmigration not only through direct adhesion, but also through the local unbuttoning of endothelial junctions. In support of this view, it is documented that LYVE-1 can transduce signals for VE-cadherin turnover and endothelial-junction remodeling in LEC-like cell lines *in vitro*[38], a process also triggered by LYVE-1 mAbs and HA binding in primary LECs (Y.J. Wang and D.G.J., unpublished observations). Although the LEC monolayers

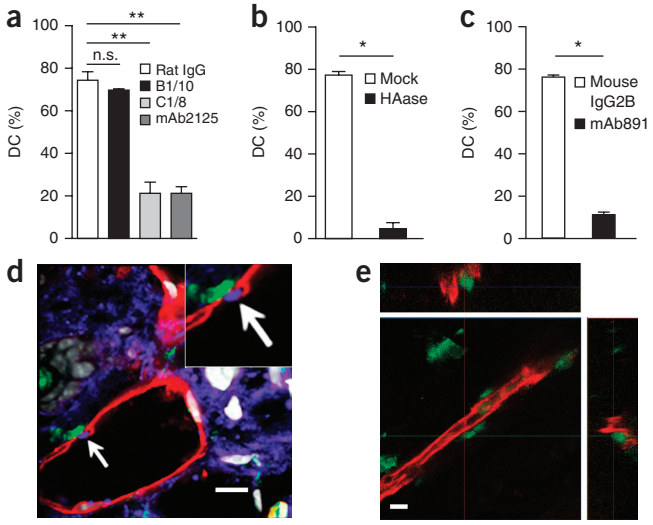

Figure 8 LYVE-1 engagement with the HA coat on DCs is required for the formation of transmigratory cups. (**a**–**c**) Quantitation of microscopy images to show the number of LYVE-1$^+$ cups associating with adherent DCs in mLEC monolayers overlaid with mouse BMDCs (**a**,**b**) after coculture and incubation in the presence of mAbs (**a**) or after 2 h of preincubation with HAase (**b**), and in human LECs with MDDCs in the presence of the HA-blocking mouse anti-human mAb 891 (**c**). Data are the mean and s.e.m. ($n = 4$) from one experiment representative of three. (**d**) Detection of HA on endogenous dermal DCs during transmigration into lymphatic vessels *in vivo*, in frozen skin sections from BALB/c mice subjected to oxazolone hypersensitization. Sections were immunostained with bVG1 (blue), anti-MHCcIII–FITC (green), and anti-podoplanin to identify lymphatic vessels (red). Scale bar, 10 µm. Inset is at 2× relative magnification. (**e**) Orthogonal view of a LYVE-1-enriched cup surrounding an individual DC, as shown in a *z*-stack of whole-mount mouse dermis immunostained with rabbit anti-LYVE-1 (red), 24 h after topical application of oxazolone and intradermal injection of CMFDA-labeled BMDCs (green). Magnification, 630×; scale bar, 20 µm. *$P < 0.03$, **$P < 0.008$, Mann-Whitney *U*-test.

used here do not spontaneously assemble interdigitating button-like junctions during *in vitro* culture and instead form continuous zipper-like junctions, these are plastic *in vivo* and can transition between the two states according to the tissue's inflammatory status[39]. Thus, the LYVE-1$^+$ transmigratory cups we observed in mouse and human LECs probably reflect authentic physiological structures. The analogous LYVE-1$^+$ membranous protrusions we observed around dermal DCs undergoing vessel entry in mouse skin lend further credence to this notion.

The role of LYVE-1 in lymphatic trafficking bears comparison with that of the closely related leukocyte HA receptor CD44, which mediates lymphocyte and neutrophil capture from laminar blood flow by engaging HA from the luminal glycocalyx in inflamed vascular endothelium[40]. Importantly, the avidity of the CD44–HA interaction necessary for such capture depends on the capacity of HA to form cross-linked complexes with inflammation-associated binding partners such as TSG-6 (ref. 41), or adduct formation with serum-derived HA-associated protein (SHAP)[21,42,43]. In lymphatic vessels, LYVE-1 must instead play a reciprocal role by engaging HA arrayed on the leukocyte surface. Although we have yet to determine whether DCs organize this surface HA in similar cross-linked complexes, it is noteworthy that they can synthesize both TSG-6 and the heavy chain of inter-α trypsin inhibitor (IαI) that generates SHAP[44,45]. Moreover, native LYVE-1 has a marked preference for binding cross-linked HA–TSG-6 complexes, which harness avidity by inducing receptor surface clustering[46]. This preference is exploited by pathogenic group A hemolytic streptococci to bind LYVE-1 through their dense HA surface capsule for enhanced dissemination to host LNs[47]. Thus the properties of LYVE-1 seem to be ideally suited for selective docking with cell-surface HA assemblages rather than free ambient HA in the tissue matrix. Indeed, LYVE-1–HA bonds form more rapidly and rupture more easily than CD44–HA bonds do in response to force, despite their similar binding affinities (K_d: 8–125 µM) (F. Bano, S.B., D.G.J. and R.P. Richter, unpublished observations), in keeping with a role in supporting DC crawling at the lymphatic vessel surface, where lower shear forces are encountered compared with those in venous blood flow[48].

Finally, although our current study highlighted the role of LYVE-1 in mediating DC entry to dermal lymphatic vessels, it is possible that the receptor also facilitates trafficking in LNs, where its location in the paracortical and medullary sinuses would suggest a role in the movement of DCs from lymph to the T-cell-rich areas. Both in nodal lymphatics and in peripheral lymphatics, LYVE-1 is likely to mediate the migration of a variety of immunomodulatory populations besides DCs. Notably, monocytes and macrophages also synthesize HA, and human monocyte-derived macrophages use LYVE-1 and HA for transmigration across LECs *in vitro*[46]. In contrast, neutrophils, which exit the skin via lymph in response to bacterial infection, do not seem to use LYVE-1 for vessel entry, and instead utilize an unusual β2-integrin- and lipoxin-mediated mechanism[49,50]. The degree of LYVE-1 involvement may well depend on the nature and extent of leukocyte HA organization and the particular choice of vessel sites targeted by these cells for entry.

In conclusion, we have shown that the LYVE-1–HA interaction constitutes a physiologically important axis that regulates DC trafficking in lymph. Consequently, LYVE-1 has potential as a therapeutic target for limiting inflammation and associated immune activation.

METHODS

Methods, including statements of data availability and any associated accession codes and references, are available in the online version of the paper.

Note: Any Supplementary Information and Source Data files are available in the online version of the paper.

ACKNOWLEDGMENTS

This work was supported by the UK Medical Research Council through MRC Human Immunology Unit core funding and Project Grant MR/L008610/1 (to D.G.J.). *Lyve1*$^{-/-}$ mice on the C57BL/6 background were kindly provided by Regeneron Pharmaceuticals (Tarrytown, New York, USA). F5 TCR-transgenic mice recognizing the H-2D^b-restricted influenza virus nucleoprotein epitope ASNENMDAM (Flu-NP$_{366–374}$) were kindly provided by D. Kioussis (National Institute of Medical Research, London, UK). CD11c–GFP reporter mice were a kind gift from F. Powrie (Kennedy Institute of Rheumatology, University of Oxford, Oxford, UK). The authors acknowledge the now deceased M. Puklavec (Sir William Dunn School of Pathology, Oxford, UK) for his invaluable technical advice on making rat monoclonal antibodies, and the Wolfson Imaging Centre, Weatherall Institute of Molecular Medicine (Oxford, UK), for access to the fluorescence microscopy equipment used in this project. The authors also thank P. Sopp, C. Waugh, K. Clark and S.-A. Clark at the WIMM Flow Cytometry Facility for their excellent technical assistance and advice.

AUTHOR CONTRIBUTIONS

L.A.J. and D.G.J. designed experiments, interpreted the data and wrote the manuscript. S.B. performed experiments, helped interpret the data and edited the manuscript. L.A.J., U.G. and G.P. performed experiments and analyzed data. W.L., K.A.H. and Y.M.R. performed experiments and provided reagents. T.H., V.C. and N.W.G. provided critical reagents and helped edit the manuscript.

COMPETING FINANCIAL INTERESTS

The authors declare no competing financial interests.

1. Mellman, I. & Steinman, R.M. Dendritic cells: specialized and regulated antigen processing machines. *Cell* **106**, 255–258 (2001).
2. Randolph, G.J., Ivanov, S., Zinselmeyer, B.H. & Scallan, J.P. The lymphatic system: integral roles in immunity. *Annu. Rev. Immunol.* **35** http://dx.doi.org/10.1146/annurev-immunol-041015-055354 (2017).
3. Miteva, D.O. *et al.* Transmural flow modulates cell and fluid transport functions of lymphatic endothelium. *Circ. Res.* **106**, 920–931 (2010).
4. Martín-Fontecha, A. *et al.* Regulation of dendritic cell migration to the draining lymph node: impact on T lymphocyte traffic and priming. *J. Exp. Med.* **198**, 615–621 (2003).
5. Lämmermann, T. *et al.* Rapid leukocyte migration by integrin-independent flowing and squeezing. *Nature* **453**, 51–55 (2008).
6. Johnson, L.A. & Jackson, D.G. Inflammation-induced secretion of CCL21 in lymphatic endothelium is a key regulator of integrin-mediated dendritic cell transmigration. *Int. Immunol.* **22**, 839–849 (2010).
7. Johnson, L.A. & Jackson, D.G. The chemokine CX3CL1 promotes trafficking of dendritic cells through inflamed lymphatics. *J. Cell Sci.* **126**, 5259–5270 (2013).
8. Kabashima, K. *et al.* CXCL12-CXCR4 engagement is required for migration of cutaneous dendritic cells. *Am. J. Pathol.* **171**, 1249–1257 (2007).
9. Jackson, D.G. Lymphatic regulation of cellular trafficking. *J. Clin. Cell. Immunol.* **5**, 258–267 (2014).
10. Russo, E. *et al.* Intralymphatic CCL21 promotes tissue egress of dendritic cells through afferent lymphatic vessels. *Cell Rep.* **14**, 1723–1734 (2016).
11. Weber, M. *et al.* Interstitial dendritic cell guidance by haptotactic chemokine gradients. *Science* **339**, 328–332 (2013).
12. Takamatsu, H. *et al.* Semaphorins guide the entry of dendritic cells into the lymphatics by activating myosin II. *Nat. Immunol.* **11**, 594–600 (2010).
13. Baluk, P. *et al.* Functionally specialized junctions between endothelial cells of lymphatic vessels. *J. Exp. Med.* **204**, 2349–2362 (2007).
14. Pflicke, H. & Sixt, M. Preformed portals facilitate dendritic cell entry into afferent lymphatic vessels. *J. Exp. Med.* **206**, 2925–2935 (2009).
15. Johnson, L.A. *et al.* An inflammation-induced mechanism for leukocyte transmigration across lymphatic vessel endothelium. *J. Exp. Med.* **203**, 2763–2777 (2006).
16. Nitschké, M. *et al.* Differential requirement for ROCK in dendritic cell migration within lymphatic capillaries in steady-state and inflammation. *Blood* **120**, 2249–2258 (2012).
17. Teijeira, A. *et al.* Lymphatic endothelium forms integrin-engaging 3D structures during DC transit across inflamed lymphatic vessels. *J. Invest. Dermatol.* **133**, 2276–2285 (2013).
18. Irjala, H. *et al.* Mannose receptor is a novel ligand for L-selectin and mediates lymphocyte binding to lymphatic endothelium. *J. Exp. Med.* **194**, 1033–1042 (2001).
19. Salmi, M., Koskinen, K., Henttinen, T., Elima, K. & Jalkanen, S. CLEVER-1 mediates lymphocyte transmigration through vascular and lymphatic endothelium. *Blood* **104**, 3849–3857 (2004).
20. Banerji, S. *et al.* LYVE-1, a new homologue of the CD44 glycoprotein, is a lymph-specific receptor for hyaluronan. *J. Cell Biol.* **144**, 789–801 (1999).
21. McDonald, B. & Kubes, P. Interactions between CD44 and hyaluronan in leukocyte trafficking. *Front. Immunol.* **6**, 68 (2015).
22. Cumberbatch, M., Dearman, R.J., Griffiths, C.E. & Kimber, I. Epidermal Langerhans cell migration and sensitisation to chemical allergens. *APMIS* **111**, 797–804 (2003).
23. Gale, N.W. *et al.* Normal lymphatic development and function in mice deficient for the lymphatic hyaluronan receptor LYVE-1. *Mol. Cell. Biol.* **27**, 595–604 (2007).
24. Prevo, R., Banerji, S., Ferguson, D.J.P., Clasper, S. & Jackson, D.G. Mouse LYVE-1 is an endocytic receptor for hyaluronan in lymphatic endothelium. *J. Biol. Chem.* **276**, 19420–19430 (2001).
25. Stoitzner, P., Romani, N., McLellan, A. & Tripp, C. Isolation of skin dendritic cells from mouse and man. *Methods Mol. Biol.* **595**, 235–248 (2010).
26. Larsen, C.P. *et al.* Migration and maturation of Langerhans cells in skin transplants and explants. *J. Exp. Med.* **172**, 1483–1493 (1990).
27. Cumberbatch, M., Dearman, R.J., Antonopoulos, C., Groves, R.W. & Kimber, I. Interleukin (IL)-18 induces Langerhans cell migration by a tumour necrosis factor-α- and IL-1β-dependent mechanism. *Immunology* **102**, 323–330 (2001).
28. Teoh, D., Johnson, L.A., Hanke, T., McMichael, A.J. & Jackson, D.G. Blocking development of a $CD8^+$ T cell response by targeting lymphatic recruitment of APC. *J. Immunol.* **182**, 2425–2431 (2009).
29. Johnson, L.A., Prevo, R., Clasper, S. & Jackson, D.G. Inflammation-induced uptake and degradation of the lymphatic endothelial hyaluronan receptor LYVE-1. *J. Biol. Chem.* **282**, 33671–33680 (2007).
30. Banerji, S., Hide, B.R., James, J.R., Noble, M.E. & Jackson, D.G. Distinctive properties of the hyaluronan-binding domain in the lymphatic endothelial receptor Lyve-1 and their implications for receptor function. *J. Biol. Chem.* **285**, 10724–10735 (2010).
31. Estcourt, M.J., McMichael, A.J. & Hanke, T. Altered primary $CD8^+$ T cell response to a modified virus Ankara(MVA)-vectored vaccine in the absence of $CD4^+$ T cell help. *Eur. J. Immunol.* **35**, 3460–3467 (2005).
32. Mummert, M.E. *et al.* Synthesis and surface expression of hyaluronan by dendritic cells and its potential role in antigen presentation. *J. Immunol.* **169**, 4322–4331 (2002).
33. Chang, M.Y. *et al.* A rapid increase in macrophage-derived versican and hyaluronan in infectious lung disease. *Matrix Biol.* **34**, 1–12 (2014).
34. de la Motte, C.A. & Drazba, J.A. Viewing hyaluronan: imaging contributes to imagining new roles for this amazing matrix polymer. *J. Histochem. Cytochem.* **59**, 252–257 (2011).
35. Clark, S.J. *et al.* Mapping the differential distribution of glycosaminoglycans in the adult human retina, choroid, and sclera. *Invest. Ophthalmol. Vis. Sci.* **52**, 6511–6521 (2011).
36. Schmits, R. *et al.* CD44 regulates hematopoietic progenitor distribution, granuloma formation, and tumorigenicity. *Blood* **90**, 2217–2233 (1997).
37. Protin, U., Schweighoffer, T., Jochum, W. & Hilberg, F. CD44-deficient mice develop normally with changes in subpopulations and recirculation of lymphocyte subsets. *J. Immunol.* **163**, 4917–4923 (1999).
38. Hou, W.H. *et al.* CRSBP-1/LYVE-1 ligands disrupt lymphatic intercellular adhesion by inducing tyrosine phosphorylation and internalization of VE-cadherin. *J. Cell Sci.* **124**, 1231–1244 (2011).
39. Yao, L.C., Baluk, P., Srinivasan, R.S., Oliver, G. & McDonald, D.M. Plasticity of button-like junctions in the endothelium of airway lymphatics in development and inflammation. *Am. J. Pathol.* **180**, 2561–2575 (2012).
40. Siegelman, M.H., DeGrendele, H.C. & Estess, P. Activation and interaction of CD44 and hyaluronan in immunological systems. *J. Leukoc. Biol.* **66**, 315–321 (1999).
41. Lesley, J. *et al.* TSG-6 modulates the interaction between hyaluronan and cell surface CD44. *J. Biol. Chem.* **279**, 25745–25754 (2004).
42. de la Motte, C.A., Hascall, V.C., Drazba, J., Bandyopadhyay, S.K. & Strong, S.A. Mononuclear leukocytes bind to specific hyaluronan structures on colon mucosal smooth muscle cells treated with polyinosinic acid:polycytidylic acid: inter-α-trypsin inhibitor is crucial to structure and function. *Am. J. Pathol.* **163**, 121–133 (2003).
43. Petrey, A.C. & de la Motte, C.A. Hyaluronan, a crucial regulator of inflammation. *Front. Immunol.* **5**, 101 (2014).
44. Maina, V. *et al.* Coregulation in human leukocytes of the long pentraxin PTX3 and TSG-6. *J. Leukoc. Biol.* **86**, 123–132 (2009).
45. Chang, M.Y. *et al.* Monocyte-to-macrophage differentiation: synthesis and secretion of a complex extracellular matrix. *J. Biol. Chem.* **287**, 14122–14135 (2012).
46. Lawrance, W., Banerji, S., Day, A.J., Bhattacharjee, S. & Jackson, D.G. Binding of hyaluronan to the native lymphatic vessel endothelial receptor LYVE-1 is critically dependent on receptor clustering and hyaluronan organization. *J. Biol. Chem.* **291**, 8014–8030 (2016).
47. Lynskey, N.N. *et al.* Rapid lymphatic dissemination of encapsulated group A streptococci via lymphatic vessel endothelial receptor-1 interaction. *PLoS Pathog.* **11**, e1005137 (2015).
48. Bano, F., Banerji, S., Howarth, M., Jackson, D.G. & Richter, R.P. A single molecule assay to probe monovalent and multivalent bonds between hyaluronan and its key leukocyte receptor CD44 under force. *Sci. Rep.* **6**, 34176 (2016).
49. Hampton, H.R., Bailey, J., Tomura, M., Brink, R. & Chtanova, T. Microbe-dependent lymphatic migration of neutrophils modulates lymphocyte proliferation in lymph nodes. *Nat. Commun.* **6**, 7139 (2015).
50. Rigby, D.A., Ferguson, D.J., Johnson, L.A. & Jackson, D.G. Neutrophils rapidly transit inflamed lymphatic vessel endothelium via integrin-dependent proteolysis and lipoxin-induced junctional retraction. *J. Leukoc. Biol.* **98**, 897–912 (2015).

ONLINE METHODS

Human and animal studies. All studies involving human tissue were approved by the Oxford Regional Health Committee (OXREC). Animal studies were carried out with appropriate UK Home Office licenses, with ethical approval from Oxford University.

Lyve1$^{-/-}$ mice on the C57BL/6 background were kindly provided by Regeneron Pharmaceuticals[23]. Mice were backcrossed for ten generations onto a BALB/c background and subsequently maintained as a heterozygous colony at Biomedical Services, John Radcliffe Hospital. F5 TCR-transgenic mice recognizing the H-2D^b-restricted influenza virus nucleoprotein epitope ASNENMDAM (Flu-NP$_{366–374}$) were kindly provided by Dimitris Kioussis (National Institute of Medical Research) and maintained at the Biomedical Services Unit (John Radcliffe Hospital, Oxford, UK). C57BL/10 and C57BL/6 mice were from Envigo RMS Inc. (Bicester, Oxfordshire, UK). OT-1 C57BL/6 TCR-transgenic mice recognizing the H-2K^b-restricted ovalbumin epitope SIINFEKL were from the Jackson Laboratory (Bar Harbor, Maine, USA). CD11c–GFP reporter mice were a kind gift from Fiona Powrie (Kennedy Institute of Rheumatology, University of Oxford). We used a total of 1,600 mice (6–8-week-old females) in the current study. All animal studies were conducted with appropriate UK Home Office licenses and with approval from the Oxford local ethics committee.

Genotyping. Ear notches from mice generated by *Lyve1*$^{-/+}$ × *Lyve1*$^{-/+}$ breeding were digested in 200 µl of DirectPCR (Tail) lysis reagent (Viagen 102-T) supplemented with Proteinase K, 0.4 mg/ml (Sigma-Aldrich P2308), for 16 h at 55 °C, then heated to 85 °C for 45 min before use in PCRs. MyTaq Red Mix (Bioline) and primers at 0.8 µM working concentrations were used, with denaturing at 94 °C for 4 min followed by 40 cycles of 94 °C for 1 min, annealing at 50 °C for 45 s and extension at 72 °C for 45 s in a Hybaid PCR machine. For 3′-end genotyping PCR we used the primers pGK.Neo.2Fw (knockout forward primer) TCATTCTCAGTATTGTTTTGCC, 3′ Lyve-F3 (wild-type forward primer) CGTGAAAAGGTGAGGTTG, and 161 SD (common reverse primer) TCACTCCTATTGAACAGTACC, which yielded PCR products of 381 bp for the knockout band and 310 bp for the wild-type band. For 5′-end genotyping PCR we used the primer 161 SU (common forward primer) GGAGGCTTCCTTACATAGAC with either LACZ.SEE-RD (knockout reverse primer) GTCTGTCCTAGCTTCCTCACTG or 5′ Lyve-R2 (wild-type reverse primer) GACAAAGGTTAGAAGGCAC, which yielded products of 556 bp for knockout and 554 bp for the wild type. Products were electrophoresed on 1.2% agarose–Tris–borate–EDTA gels.

Antibodies. Rat anti-mouse LYVE-1 (mAb2125) was from R&D Systems; mAbs B1/10 and C1/8 were generated previously, with mouse LYVE-1 Fc used as the immunogen[28,29], as was polyclonal rabbit anti-LYVE-1 (ref. 20). Rat IgG fractions were purified from hybridoma supernatants with Protein G–Sepharose. Other antibodies used were mouse anti-human LYVE-1 (R&D Systems; clone 891), goat anti-mouse podoplanin (R&D Systems; AF3244), hamster anti-mouse podoplanin (eBioscience; 14-5381-85; clone 8.1.1), rat anti-mouse CD31 (clone MEC 13.3; BD Pharmingen), rat anti-mouse VE-cadherin (clone 11D4.1; BD Pharmingen) and rat anti-mouse ICAM-1 (YN1/1.7.4) (hybridoma cultured in-house, purified with Protein G–Sepharose and as used previously in ref. 15). All antibodies were used at 10 µg/ml for immunostaining and 50 µg/ml for function-blocking. Biotinylated hyaluronan-binding protein (recombinant human versican G1 domain, bVG-1, AMSBio, AMS.HKD-BC41) was used at 3 µg/ml and detected with either streptavidin-conjugated Alexa Fluor 647 or streptavidin-conjugated Alexa Fluor–Pacific Blue. All secondary conjugates (Alexa Fluor 488, 546, 594 and 647) were from Molecular Probes, Invitrogen. IgG isotype controls were from R&D Systems. The following mouse antibodies were used for flow cytometry: anti-CD11c–phycoerythrin (PE)/Cy7 (BioLegend; 117318; clone N418), anti-CD11b–BUV395 (BD Biosciences; 563553; clone M1/70), anti-MHCII (I-A/I-E)–eFluor450 (eBioscience; 48-5321-82; clone M5/114.15.2), anti-CD45–BV785 (BioLegend; 103149; clone 30-F11), anti-EpCAM–BV605 (BioLegend; 118227; clone G8.8), anti-langerin–PE (eBioscience; 12-2075-82; clone eBioL31), anti-CD103–allophycocyanin (eBioscience; 17-1031-82; clone 2E7), anti-F4/80–PE/Cy5 (BioLegend; 123112; clone BM8), and anti-CD86–PE (BD Pharmingen; 553692; clone GL1). All antibodies that were used for functional assays (both *in vivo* and *in vitro*) were tested for endotoxin contamination with a Pierce LAL chromogenic endotoxin quantitation kit (Thermo Fisher Scientific; 88282) according to the manufacturer's protocol, to ensure that endotoxin levels were less than 10 pg/ml.

Cells. Primary mouse and human lymphatic endothelial cells were prepared from freshly resected skin samples by immunoselection with LYVE-1 mAb and MACS beads (Miltenyi Biotec) as described[15]. BMDCs were extracted from tibia and fibula bones of euthanized mice, passed through a 70-µm cell strainer, and cultured for 7 d in DC medium (RPMI 1640 medium with 10% FCS, kanamycin sulfate, MEM nonessential amino acids, sodium pyruvate, glutamine, 2-mercaptoethanol (55 mM) (all Life Technologies), and supplemented with recombinant mouse GM-CSF and IL-4 (20 ng/ml, premium grade; Miltenyi Biotec)). The CD11c$^+$MHCclII$^+$ phenotype was routinely confirmed by flow cytometry (**Supplementary Fig. 5a**). Human monocytes were purified from peripheral blood mononuclear cells from healthy donors by positive immunoselection with anti-CD14-conjugated MACS beads (Miltenyi Biotec). We generated DCs by culturing monocytes for 5 d in DC medium supplemented with recombinant human GM-CSF (50 ng/ml) and 10 ng/ml IL-4 (premium grade; Miltenyi-Biotec). Non-adherent DCs were matured with 1 µg/ml LPS from *Salmonella abortus* (Sigma-Aldrich) and labeled with CMFDA Cell Tracker Green (Invitrogen) according to the manufacturer's protocol. Jurkat E6.1 cells were purchased from Sigma and tested in-house to ensure that there was no mycoplasma contamination.

Migration of DCs after oxazolone sensitization and FITC painting. For measurement of endogenous dermal DC trafficking, we sensitized 8-week-old *Lyve1*$^{-/-}$ C57BL/6 or BALB/c mice or *Lyve1*$^{+/+}$ littermate controls by topical application of 3% (wt/vol) oxazolone (4-ethoxymethylene-2 phenyl-2-oxazoline-5-one; Sigma-Aldrich; E0753) + 4 mg/ml FITC (fluorescein isothiocyanate isomer 1; Sigma-Aldrich; F7250) in 95% aqueous ethanol to the shaved abdomen (150 µl per mouse). Where appropriate, C1/8, B1/10 or mAb2125 (0.5 mg/mouse) was administered by i.p. injection 24 h before application of oxazolone and FITC. To assess the effects of anti-LYVE-1 mAbs on the challenge phase of contact hypersensitivity, we sensitized mice by topical application of 3% (wt/vol) oxazolone in 95% aqueous ethanol to both ears (50 µl per ear) on days 0 and 1, administered i.p. injections of mAbs on day 5, and then applied a second topical dose of oxazolone and FITC (0.8% oxazolone (wt/vol) + 4 mg/ml FITC; 150 µl per mouse) to the shaved abdomen on day 6. We killed the mice on day 7.

For trafficking of adoptively transferred BMDCs, mice were sensitized and challenged with oxazolone to increase mobilization essentially as described above, except that oxazolone was applied to the abdomen rather than the ears, and the CMFDA-labeled BMDCs (1×10^6) were injected intradermally at the same time as oxazolone challenge, 24 h after i.p. injection of anti-LYVE-1 blocking mAbs (0.5 mg per mouse) where indicated.

***Ex vivo* DC crawl-out assays from mouse ear explants.** After the mice had been killed, we removed the ears from naive mice, peeled them into dorsal and ventral halves, and cultured them for 24 h (exposed-dermis-side down) in 24-well dishes in RPMI 1640 medium supplemented with 10% FCS, penicillin–streptomycin and glutamine (Life Technologies), and mouse TNF, 50 ng/ml (R&D Systems). After culture, dermal sheets were removed and digested in Collagenase P (0.2 mg/ml; Roche; 11213865001) and Dispase, 0.8 mg/ml (Life Technologies; 17105-041) in RPMI medium at 37 °C for 30 min, then mechanically disrupted through a 100-µm cell strainer before being stained alongside egressed cells for flow cytometry.

To investigate the effects of anti-LYVE-1 mAbs on the ability of DCs to egress from ear dermis, we administered mAbs to live naive mice by i.p. injection (0.5 mg). 24 h later, we killed the mice and cultured dermal sheets in the presence of mouse TNF, 50 ng/ml, and appropriate mAbs (50 µg/ml) for a further 24 h.

Removal of surface HA from BMDCs for adoptive transfer. Nonadherent BMDCs were incubated with 15 U/ml hyaluronidase (from *Streptomyces hyalurolyticus*; Sigma-Aldich) for 2 h at 37 °C in DC medium, then washed and replated in DC medium supplemented with 25 mM HEPES (Life Technologies) and 4-methylumbelliferone (7-hydroxy-4-methylcoumarin) sodium salt (4-MU; Sigma-Aldrich; M1508; 0.1 mM dissolved in ddH_2O) for 72 h.

We induced maturation by adding 1 μg/ml LPS during the final 24 h of incubation. Control (untreated) BMDCs were mock-treated in parallel with the hyaluronidase- and 4-MU treated cells. Nonadherent cells were then labeled with either Qtracker 655 (Q25021MP) or Qtracker 585 (Q25011MP) cell-labeling kits, according to the manufacturer's protocol, and then washed and mixed 1:1 before intradermal coinjection into the ears of oxazolone-sensitized mice. We used 0.5×10^6 cells from mock-treated mice and 0.5×10^6 cells from hyaluronidase- and 4-MU-treated mice per injection.

MVA.HIVA.NP-specific lymph node T cell response model. Lymphocytes were isolated from F5 transgenic mice, labeled with 5.5 μM CFSE (Molecular Probes, Invitrogen), resuspended in endotoxin-free PBS, and injected intravenously into sex- and age-matched naive C57BL/10 mice (2×10^6 cells per mouse). After 24 h, we administered 0.5 mg of rat IgG, mAb B1/10 or mAb C1/8 by i.p. injection to these F5-BL10 chimeras. After another 24 h, we immunized the chimeras with 2×10^6 plaque-forming units of recombinant modified vaccinia virus Ankara expressing flu-$NP_{366–374}$ (MVA.HIVA.NP) intradermally or, in the case of controls used for spleen T cell proliferation, via an intravenous route. mAbs were administered again 24 h after MVA.HIVA.NP injection, and mice were killed 48 h after that (i.e., 3 d after MVA.HIVA.NP vaccination). We removed draining cervical LNs and spleens and obtained single-cell suspensions in FACS incubation buffer (PBS + 1% FCS, 0.01% sodium azide), then stained them for NP-specific $CD8^+$ T cells using human influenza virus A–$NP_{366–374}$-specific tetramer (1/160 dilution)[28] and PerCP-conjugated anti-CD8α mAb (1/150 dilution; BD Biosciences). Cells were washed twice in FACS buffer, then resuspended in CellFix (BD Biosciences). For analysis by flow cytometry, cells were gated according to forward-scatter, side-scatter and pulse width to yield singlets, then by detection of CD8 and NP.

Ovalbumin-specific lymph node T cell response model. $CD8^+$ lymphocytes were isolated from C57BL/6 OT-1 transgenic mice and purified by negative immunomagnetic bead selection (Miltenyi-Biotec) before being labeled with 5 μM CFSE (Molecular Probes, Invitrogen). Cells were then washed in endotoxin-free PBS and injected intravenously into naive sex- and age-matched C57BL/6 *Lyve1*$^{-/-}$ mice and *Lyve1*$^{+/+}$ littermate controls (4×10^6 cells per mouse). The following day, BMDCs (prepared from age- and sex-matched C57BL/6 mice as described above) were incubated for 1 h in the presence of ovalbumin peptide SIINFEKL (1×10^{-7} M) and LPS (1 μg/ml), then washed four times in PBS and injected intradermally into the ears of the OT-1 chimeras (0.5×10^6 BMDCs per ear). Mice were killed 44 h later; draining cervical LNs and nondraining inguinal LNs were removed, passed through 100-μm cell strainers to yield single-cell suspensions, and stained for OT-1-specific $CD8^+$ T cells with tetrameric H-2 K^b/$OVA_{257–264}$ peptide complexes conjugated with allophycocyanin, anti-CD8–BV421, anti-CD25–PerCPCy5.5 and anti-CD69–PE/Cy7, in the presence of TruStain fcX (anti-mouse CD16/CD32 clone 93; BioLegend) Fc blocker. Finally, cells were incubated with Live-Dead Near-IR dead cell stain (Thermo Fisher Scientific). For analysis by flow cytometry, cells were gated according to forward- and side-scatter to yield singlets, then by detection of live dye-excluding cells, which were further characterized by expression of CD8 and detection of ovalbumin peptide by tetramer.

Flow cytometric analysis of LNs. LNs from either naive or topical-oxazolone-hypersensitized mice were cut in half and digested for 37 °C in Collagenase D (Roche; 11088882001), 1 mg/ml (wt/vol), in RPMI 1640 medium, then mechanically disrupted through a 100-μm cell strainer. Cells were suspended in incubation buffer (PBS + 10% FCS, 0.01% azide) and maintained on ice for all subsequent incubation steps. Cells were incubated first with Fixable Viability Dye eFluor780 (eBioscience; 65-0865) for 15 min, then with TruStain FcX (anti-mouse CD16/CD32; clone 93; BioLegend) Fc blocker for 15 min, and finally with fluorescently conjugated antibodies for 20 min. Cells were then washed and incubated for 15 min in IC fixation buffer (eBioscience; 00-8222-49) before being washed in permeabilization buffer (eBioscience; 00-8333-56) and stained with anti-langerin–PE. We carried out staining with recombinant biotin-labeled versican G1 domain (bVG1) (biotinylated hyaluronic-acid-binding protein AMS.HKD-BC41 from AMS Biotechnology (Europe) Ltd) after all other incubations by fixing the cells in 2% formaldehyde (vol/vol) for 5 min, then incubating them with 3 μg/ml bVG1 for 40 min followed by streptavidin–Alexa Fluor 647 (Life Technologies; S21374) for 40 min.

Cells were counted either manually or with 123count eBeads (eBioscience; 01-1234-42) and analyzed with a flow cytometer (CyAn, Beckman Coulter, or LSRII, BD Biosciences) and Flow-Jo software. Compensation was carried out with anti-mouse immunoglobulin/negative-control compensation particle set beads (BD CompBeads; 552843) and fluorescence-minus-one controls. As a control for nonspecific binding of bVG1, samples were treated with hyaluronidase (see below) before immunostaining.

Immunofluorescent antibody staining of cells and tissues. Monolayers of cells cultured in eight-chamber slides (BD Falcon) were fixed in paraformaldehyde (1% wt/vol in PBS, pH 7.4) for 5 min and washed in PBS, and then primary antibodies were applied in blocking buffer (PBS + 1% BSA + 10% FCS). Cells were incubated at room temperature for 45 min, washed, and further incubated for 30 min with Alexa Fluor–conjugated secondary antibodies before being mounted in Vectashield + DAPI (Vector Laboratories; H-1200) and viewed on a Zeiss LSM 780 confocal microscope. Images were captured by sequential scanning, with no overlap in the detection of emissions from each fluorophore, with a 10×/0.3 DIC M27 Plan-Apochromat (total magnification: 100×), a 40×/1.1-NA W Korr UV-Vis-IR LDC-Apochromat (total magnification: 400×), or a 63×/1.4-NA oil-immersion Plan-Apochromat (total magnification, 630×; resolution, 0.24 μm).

For whole-mount staining, mouse dermis was fixed in 1% paraformaldehyde for 1 h, washed in PBS–Triton X-100 (0.3% vol/vol), blocked with BSA (1% wt/vol) and FCS (10% vol/vol), and incubated with primary antibodies at 4 °C overnight and fluorescently labeled secondary antibodies at 2 h at room temperature. Tissue samples were then mounted in Vectashield (Vector Laboratories H-1000) and viewed by confocal microscope. When staining tissue to detect transmigratory cups, we left the tissue non-permeabilized, omitting Triton X-100.

For the preparation of thin frozen sections, we froze tissues in OCT embedding medium (R. A. Lamb Laboratory Supplies) and then cut 8-μm sections with a cryostat. Primary antibodies and, subsequently, Alexa Fluor conjugates were applied before samples were mounted in Vectashield and viewed by confocal microscope.

LEC–DC adhesion and transmigration assay. To quantify adhesion, we layered confluent monolayers of primary mLECs in gelatin-coated 24-well dishes with 5×10^5 fluorescently labeled LPS-matured BMDCs per well and incubated them at 37 °C for 3 h. We measured the total number of DCs present with a fluorescence plate reader. We then gently rinsed the cells (three times with PBS) to remove nonadherent DCs before re-measuring fluorescence and calculating the percentage of adherent cells. To assess the effect of LYVE-1-blocking mAbs, we pre-incubated the monolayers (30 min, 37 °C) with LYVE-1 mAbs or control immunoglobulin as appropriate before layering them with BMDCs. To remove HA from cell surfaces before assaying for adhesion, we pre-incubated cells with 15 U/ml hyaluronidase (from *S. hyalurolyticus*; Sigma-Aldich) for 2 h at 37 °C, then washed them in medium.

For measurement of transmigration, primary mLECs were seeded onto the underside of gelatin-coated Fluoroblok cell culture inserts (3-μm pore size; BD Falcon) and cultured in companion plates until fully confluent. Monolayers were then pre-incubated (37 °C, 30 min) with LYVE-1-blocking mAbs or control immunoglobluin as appropriate before the addition of 5×10^5 fluorescently labeled LPS-matured BMDCs per well, and transmigration assays were carried out as described[15] with a fluorescence plate reader (Synergy HT, Bio-Tek) at 37 °C.

Quantitation of LYVE-1$^+$ endothelial cup formation. Primary mLECs were seeded in eight-chamber slides and cultured until confluent. Antibodies were applied 30 min before the addition of 0.1×10^6 fluorescently labeled LPS-matured BMDCs per chamber. Cells were incubated at 37 °C for 3 h; then nonadherent DCs were removed by gentle washing with PBS before being immunostained as detailed above. Adherent DCs from ten fields of view per chamber were counted and scored either alone or in association with LYVE-1$^+$ cups.

doi:10.1038/ni.3750

Quantitation of DC hyaluronan levels. We used a hyaluronan ELISA kit from Echelon Biosciences according to the manufacturer's protocol. We prepared BMDCs from three *Lyve1*$^{+/+}$ BALB/c mice as described above, transferring nonadherent cells to fresh tissue-culture ware and culturing them for 24 h with or without LPS (1 μg/ml) in five replicate wells of six-well dishes. Cells were counted, and then supernatants were applied directly to the assay. Cells were lysed (150 μl per well) in lysis buffer (50 mM Tris, pH 7.5, 100 mM NaCl, 1% NP-40 and 1 mM EDTA), and debris was removed by centrifugation (1,500 r.p.m. for 5 min) before application to the assay. The HA concentration was determined in nanograms per milliliter per cell.

Characterization of LYVE-1–HA-blocking mAbs and epitope mapping. For quantitative receptor-binding analyses, mouse LYVE-1 mAbs B1/10, C1/8 and mAb2125 (0–5 μg/ml) were titrated individually against either soluble mouse LYVE-1 full-ectodomain Fc fusion protein or Jurkat T cells lentivirally transduced with full-length mouse LYVE-1 cDNA by microtiter plate binding assay and flow cytometry, respectively, essentially as described[13,46]. For comparison of potencies in HA-binding blockade, the same mouse LYVE-1 lentivirally transduced Jurkat cells were subjected to high-molecular-weight biotinylated-HA-binding assays in the presence or absence of individual LYVE-1 mAbs (0–100 μg/ml), detected with streptavidin–Alexa Fluor 485 by flow cytometry. For epitope analyses, we titrated each LYVE-1 mAb against a panel of full-length mouse LYVE-1 site-directed mutants in transfected HEK 293T cells, targeting individual amino acids equivalent to those identified as HA-binding residues in the human LYVE-1 Link module, with correction for variation in surface expression and quantitation by flow cytometry[30].

Analysis of HA synthase expression by RT-PCR. Total cellular RNA was isolated from LPS-matured BMDCs (RNeasy, Qiagen), and first-strand cDNA synthesis was carried out by Oligo dT priming using MMLV reverse transcriptase (Epicentre, Illumina Inc), according to the manufacturers' instructions. *Has2* transcripts were amplified with the primer pair mHAS2Fwd (5-GTTTTGGTGACGACAGGCAC-3) and mHAS2Rev (5-TTCCGCCTGCCACACTTCTT-3) and MyTaq Red Mix PCR (Bioline), with denaturing at 94 °C for 1 min, annealing at 55 °C for 2 min and extension at 72 °C for 2 min. Products were resolved on 1.2% agarose Tris–Borate–EDTA gels, alongside 100-bp DNA ladders (New England BioLabs).

Data and statistical analyses. Data were analyzed with Excel (Microsoft), and the Mann–Whitney *U* test was used to compare data sets throughout this study, unless otherwise stated, with Graph Pad Prism. $P < 0.05$ was considered significant. A computer-generated model of LYVE-1 was produced with the ModWeb program (https://modbase.compbio.ucsf.edu/scgi/modweb.cgi).

Data availability. The data that support the findings of this study are available from the corresponding author upon request.